Available online at www.sciencedirect.com
ScienceDirect
Acta Biomaterialia 5 (2009) 3178–3191
Acta BIOMATERIALIA
www.elsevier.com/locate/actabiomat

The effect of surface treatment on the surface texture and contact angle of electrochemically deposited hydroxyapatite coating and on its interaction with bone-forming cells

Noam Eliaz [a,*], Sharon Shmueli [a], Irena Shur [b], Dafna Benayahu [b], Daniel Aronov [c], Gil Rosenman [c]

[a] *Biomaterials and Corrosion Laboratory, School of Mechanical Engineering, Tel-Aviv University, Ramat Aviv, Tel-Aviv 69978, Israel*
[b] *Department of Cell and Development Biology, Sackler Faculty of Medicine, Tel-Aviv University, Ramat Aviv, Tel-Aviv 69978, Israel*
[c] *School of Electrical Engineering, Tel-Aviv University, Ramat Aviv, Tel-Aviv 69978, Israel*

Received 2 February 2009; received in revised form 26 March 2009; accepted 1 April 2009
Available online 10 April 2009

Abstract

This work demonstrates the effects of both surface preparation and surface post-treatment by exposure to electron beam on the surface texture, contact angle and the interaction with bone-forming cells of electrochemically deposited hydroxyapatite (HAp) coating. Both the surface texture and the contact angle of the ground titanium substrate changed as a result of either heat treatment following soaking in NaOH solution or soaking in H_2O_2 solution. Consequently, the shape of the current transients during potentiostatic deposition of HAp changed, and the resulting coatings exhibited different surface textures and contact angles. The developed interfacial area ratio *Sdr* and the core fluid retention index *Sci* were found more reliable than the mean roughness R_a and the root-mean-square roughness Z_{rms} in correlating the adhesion of the coating to the metal substrate and the cellular response with surface texture. The NaOH pretreatment provided the highest surface area and induced the highest cell attachment, even though the H_2O_2 treatment provided the highest hydrophilicity to the metal substrate. Electrodeposition at pH 6 was found preferable compared to electrodeposition at pH 4.2. The ability to modify the cellular response by exposure to unique electron-beam surface treatment was demonstrated. The very high hydrophilicity of the as-deposited HAp coating enhanced its bioactivity.

Keywords: Hydroxyapatite coating; Electrochemistry; Surface texture; Contact angle; Cell attachment; Titanium

1. Introduction

A key factor for successful fixation of cementless implants used for joint reconstruction is the establishment of a stable interface between the implant and bone. Coating of the implant with osteoconductive hydroxyapatite (HAp, $Ca_5(PO_4)_3(OH)$) is a well-known method for achieving such fixation [1]. The coating can improve the biocompatibility of orthopaedic implants by blocking the diffusion of poisonous elements from the metal into the body, as well as reducing the friction coefficient between the implant and its biological surroundings [2]. HAp is capable of enhancing bone growth across a gap around an implant in both stable and unstable mechanical conditions, and even converting a motion-induced fibrous membrane into a bony anchorage [3,4].

Several methods are available for the application of HAp coatings onto metal substrates. While plasma spraying is by far the most commonly used technique for orthopaedic implants, other techniques such as dip coating, sputtering, sol–gel, electrophoretic deposition and electrochemical deposition have attracted much interest in recent years. Because the thermal expansion coefficients of HAp

* Corresponding author. Tel.: +972 3 6407384; fax: +972 3 6407617.
E-mail address: neliaz@eng.tau.ac.il (N. Eliaz).

1742-7061/$ - see front matter © 2009 Acta Materialia Inc. Published by Elsevier Ltd. All rights reserved.
doi:10.1016/j.actbio.2009.04.005

or tricalcium phosphate (TCP, $Ca_3(PO_4)_2$) are larger than those of Ti-based metals ($11–15 \times 10^{-6}$ vs. $8–10 \times 10^{-6}$ cm cm^{-1} K^{-1}, respectively), it is not easy to obtain good coatings on metals by processes that involve high temperatures [5].

Eliaz et al. [6–13] have reviewed the advantages of electrodeposition of HAp and studied different aspects of electrocrystallization of HAp on commercially pure Ti (CP-Ti) and Ti–6Al–4V, including the effects of bath pH and operating conditions, nucleation and growth, structure, chemistry and surface morphology, corrosion behaviour and in vivo performance. In one of these studies [7], the need for improving the adhesion of the coating to the substrate, on one hand, and accelerating the bone growth during the first few days post-operation, on the other hand, was noted.

Certain surface treatments of the titanium substrate may allow these two goals to be achieved. For example, it has been reported that after soaking in an alkaline solution (e.g. 5 M NaOH at 60 °C for 24 h), a hydrated titanium oxide gel layer containing Na^+ ions is formed on the surface. A complementary heat treatment (e.g. 600 °C for 1 h) then dehydrates and densifies this layer, transforming it to amorphous sodium titanate with a porous network structure [13–18]. This phase is a precursor for amorphous calcium titanate, which induces nucleation of amorphous calcium phosphate, and then HAp. It was reported that NaOH treatment prior to electrodeposition in a modified simulated body fluid resulted in both a denser and a more uniform brushite ($CaHPO_4{\cdot}2H_2O$)/HAp coating [18]. It was speculated that the porous network of the titanium surface formed after the NaOH pretreatment provided more favourable sites for the nucleation of CaP. Soaking in NaOH per se has recently been found to be beneficial both with respect to improving the adhesion of the coating to the substrate and enhancing the bone growth around HAp-coated implants in rabbits [13].

Another treatment of the titanium substrate may be soaking in H_2O_2 [19–21], which results in formation of a relatively thick porous oxide layer on the titanium surface. In an aqueous medium, OH^- bonds to the Ti cation in TiO_2, forming Ti–OH groups, which may be either acidic or basic, depending on the pH of the electrolyte. Application of cathodic potential results in a relatively high concentration of OH^- ions in the vicinity of the cathode surface, thus locally increasing the pH and providing better conditions for the nucleation and growth of HAp.

Post-treatment of the HAp coating may also improve the cellular response. For example, the wettability and electric charge at a material surface affect both cell and bacterial adhesion. Cell adhesion, e.g. in the case of osteoblasts, is often better on hydrophilic surfaces [22,23]. There are several techniques for altering surface wettability, such as deposition of self-assembled monolayers [24], light-induced changes [25] and electrochemical methods [26]. In the present work, an innovative process was evaluated. In this treatment [27–31], low-energy electron irradiation leads to surface energy modification on the nanoscale. HAp is a *p*-type wide-band-gap semiconductor with originally positive surface band-bending and several electron/hole bulk and surface states. The energy of the primary incident electrons significantly exceeds the mobility gap in HAp ($E_g \sim 4$ eV), resulting in generation of electron–hole pairs. The traps of different origin located in the irradiated surface region lead to the capture of primary and secondary electrons and holes, which are thermalized on the scale of tens of angstroms. Because the electron mobility is higher than the hole mobility, holes may constitute hole surface traps, while electrons are localized by bulk states, thus creating a thin charged double layer near the surface (~0.5–5 nm deep). Consequently, the wettability is changed even without applying external electric fields or interlayer deposition. This process provides gradual modulation of the wettability over a wide range of contact angles, from hydrophilic to superhydrophobic, by variation of the incident electron charge. The process allows induction of either uniform or patterned wettability, without altering the topography, roughness or the phase state of the material. The tailored wettability state remains stable for at least one month in various environment conditions, such as air and high humidity. The process is reversible; the charge can be discharged by UV irradiation.

The objective of this work was to determine the effects of these three surface treatments (i.e. two pre-treatments and one post-treatment) on the surface texture, wettability and interaction with bone-forming cells in vitro of electrochemically deposited HAp.

2. Materials and methods

2.1. Sample preparation and electrodeposition

The substrate metal was CP-Ti Gr. 2, in the form of 5 mm thick sheet. Samples, 1×1 cm^2 in size, were cut and ground mechanically on SiC papers from P120 to P1000 grit. They were then washed with detergent and water, ultrasonically cleaned in acetone, recleaned ultrasonically in Millipore deionized (Milli-DI) water and dried in warm air.

Electrodeposition was carried out for 2 h at 90 °C, in a solution containing calcium nitrate $Ca(NO_3)_2$ and ammonium dihydrogen phosphate $NH_4H_2PO_4$, following the procedure described in detail elsewhere [11]. First, the effect of the initial bath pH was sought, therefore comparison was made between coatings deposited at either $pH_0 = 4.2$ or $pH_0 = 6.0$ (hereafter termed HAp4.2 and HAp6.0, respectively). The pH was measured by an InoLab pH/Oxi Level 3 meter (WTW), after the desired temperature had been attained. An EG&G/PAR 263A potentionstat/galvanostat was employed to maintain the cathode potential at −1.4 V vs. a saturated calomel electrode (SCE). The CorrWare/CorrView (v. 2.6b) software package from Scribner Associates was used for data acquisition and data analysis.

2.2. Sample pre-treatments

Following sample preparation as described in Section 2.1, some samples were left in the as-ground condition while other samples were also treated before deposition with either NaOH or H_2O_2. The NaOH treatment consisted of soaking the samples in 5 M NaOH solution at 60 °C for 24 h, washing in Milli-DI water, drying in warm air and annealing in an air furnace at 600 °C for 1 h. The H_2O_2 treatment consisted of immersion in 5 M H_2O_2 solution (30 mL) at 60 °C for 24 h, washing in Milli-DI water and drying in warm air. All pretreated samples were subsequently electrodeposited for 2 h at $E = -1.4$ V vs. Ag/AgCl in a solution at 70 °C and $pH_0 = 6.0$.

2.3. HAp surface post-treatment

The electron irradiation system employed a commercially available electron gun (EFG-7, Kimball Physics Inc., USA). The treatment was performed in vacuum of 10^{-7} Torr at room temperature, using electron flux with excitation energy between several tens of eV and 100 eV, and electron current density between 10 and 100 nA cm^{-2}. The exposure time was varied in the range of 0–3000 s, depending on the desired water contact angle. The same technique was applied to some uncoated titanium samples, in order to make them either more hydrophobic or more hydrophilic. In order to form a more hydrophilic state, UV illumination was applied, using a non-filtered UV light (185–2000 nm) and a 200 W mercury–xenon lamp.

2.4. Contact angle measurements

Sessile drops of DI water at pH = 5.5 were placed on the sample surface. The effect of surface heterogeneity of the studied samples was examined by measuring the contact angle hysteresis, using the tilting plate technique. The contact angle hysteresis is the difference between the advancing and the receding contact angles [32]. The optical wettability inspection was performed by a light microscope (Olympus MX-50, Opelco, USA), combining two CCD color cameras and image analysis by means of ImageJ 1.34s software. The volume of each drop was 2 μL. All measurements were carried out at 26 ± 1 °C and 45 ± 5% RH, with an accuracy of ±1°. The contact angles were measured 10 s after the drop was deposited, which was the estimated time required to attain equilibrium with the liquid in use. The contact angle hysteresis was 5 ± 1° for the hydrophilic state, and 17 ± 3° for the hydrophobic state.

2.5. Cell culture, fixation and counting

We used mouse osteogenic cell line MBA-15, which expresses osteoblastic phenotype in vitro and forms bone in vivo [33,34]. On each Ti sample, either coated or uncoated, 7000 cells were seeded. Cells were grown in Dulbecco's modified Eagle's minimal essential medium (DMEM, Beit Haemeck), with 10% fetal calf serum (FCS, Biological Industries), 1% glutamine (Sigma–Aldrich Ltd.), and 1% antibiotics (penicillin and streptomycin, Sigma–Aldrich Ltd.) in 5% CO_2 at 37 °C for 24 h.

The subsequent fixation procedure consisted of the following steps [35]. The specimens were washed twice by phosphate-buffered saline (PBS) and fixed in PBS containing 3% glutaraldehyde for 1 h. Then, the samples were washed three times in PBS and were immersed overnight in PBS containing 5.4% sucrose. Dehydration was performed in increasing concentrations of ethanol (from 30% to 100%), 10 min in each solution. The samples were dried for 30 min at room temperature.

Cell count was based on incorporation of 1 mg mL^{-1} BisBenzimide Hoechst 33342 trihydrochloride (Sigma–Aldrich Ltd.) that labels the DNA and serves for visualization of nuclei. This fluorescent dye was added for 5 min to cells that were then washed and post-fixed in 3% glutaraldehyde for 1.5 h. Fluorescence was recorded using a Leica DMRB upright microscope, excitation filter BP 340-380, with a magnifier 12-bit color CCD camera. Cell counting was done using ImageJ 1.34s image analysis software.

2.6. Statistical analysis

The texture, contact angle and cell count values are reported as means ± standard deviation. A one-way analysis of variance (ANOVA) and Tukey post hoc (multiple comparisons) test were applied, using the SPSS statistical package. Differences of $P < 0.05$ were considered to be statistically significant.

2.7. Characterization of surface morphology and texture

The surface morphology of gold-sputtered deposits was imaged by scanning electron microscopy (SEM, JEOL JSM-6300). The attached energy-dispersive spectroscopy (EDS, Oxford Isis) system was used to estimate the Ca/P ratio as well as to identify other elements present in the deposit. Complementary imaging was performed by environmental SEM (ESEM, Quanta 200 FEG, FEI) without any sputtering of conductive material.

Atomic force microscopy (AFM, PicoSPM™, Molecular Imaging) was used to image the surfaces in air. Imaging was done under contact mode, using tips made of Si_3N_4 (Veeco). Topography, deflection and three-dimensional images were acquired. The mean length and mean width of the CaP crystals were determined by direct measurement of features on the deflection image. The mean thickness, on the other hand, was determined from line scans on the topography image. Roughness parameters were calculated following image processing with the aid of SPIP™ software.

3. Results

3.1. Electrodeposition at pH 4.2 vs. at pH 6.0

SEM images (not shown here) revealed significant differences in the surface morphology of HAp4.2 and HAp6.0 coatings. EDS analysis revealed only reflections of Ca, P and O from the coating, and Ti (and possibly some O) from the substrate. There was no indication of the presence of other elements, such as heavy metals, in the range of 0–20 keV. The calculated Ca/P atomic ratios were 1.58 and 1.41 for HAp6.0 and HAp4.2, respectively. X-ray diffraction revealed, in both cases, only reflections of HAp (JCPDS file #09-0432) and Ti (#44-1294). Preferred orientation of both the substrate and the coating along the {0 0 2} planes was observed, as reported earlier [11]. The texture was less prominent in HAp4.2 than in HAp6.0. The latter exhibited sharper and narrower peaks, indicating that the level of crystallinity in HAp6.0 was higher than that in HAp4.2. The Debye–Scherrer equation also indicated that HAp6.0 coatings were closer to the ideal structure than HAp4.2 coatings. Other differences between the two types of coatings have been reported elsewhere [11].

In order to decide whether the focus should be on HAp4.2 or on HAp6.0 coatings, the viability of cells on each of the two surfaces was evaluated by SEM and compared to that on ground Ti (Gr-Ti). The coated samples had been masked at one corner during electrodeposition. Therefore, cells at this corner were later exposed to pure Ti. Fig. 1 demonstrates the typical MBA-15 cell coverage and cell morphology on each of the three surfaces. The area covered with cells was larger on HAp6.0 than on HAp4.2, implying that the former was more bioactive. Cell coverage over the centre of the surfaces was more prominent on Gr-Ti and on HAp6.0 than on HAp4.2 surfaces. On Gr-Ti (Fig. 1a), a confluent cell layer covered the surface, masking most of the grinding grooves. The cells were flattened and well spread, forming network, with almost no filopodia and lamellipodia visible. A correlation was observed between the orientation of the grooves and the orientation of the cells, a phenomenon known as "contact guidance" [36,37]. The cells spread much less on HAp4.2 and mostly had a stellate shape (Fig. 1b). Some cells retained the ellipsoid shape of the nucleus, with a diameter of ~7 μm, while beginning to form circular lamellipodia and spidery filopodia (Fig. 1f). Fewer rounded cells were observed on HAp6.0 (Fig. 1g) compared to HAp4.2. Instead, the cells were highly stretched on top of needles of the HAp coating and exhibited many focal contacts (Fig. 1c–e). At high magnifications (Fig. 1e), the cytoplasmic membrane seemed to be very thin, bridging over the coating protrusions, except where filopodia penetrated into pores and grasped the needles to assist in stretching and morphological changes of the cell.

Based on the higher crystallinity of HAp6.0 compared to HAp4.2, which may result in enhanced longevity of the former in vivo, and on the better cell viability on the former, it was concluded that HAp6.0 may be more attractive for orthopaedic implants. Therefore, the rest of the work was conducted on HAp6.0.

3.2. The effect of pretreatments on the surface characteristics of uncoated titanium

The appearance of the titanium surface was significantly altered by the different pretreatments, as evident from Fig. 2. Deformation and grooves due to mechanical grinding were evident on Gr-Ti (Fig. 2a). After NaOH treatment (denoted hereafter as NaOH-Ti), the grinding grooves were no longer evident, but instead the surface contained "mud cracks" that had probably formed during dehydration (Fig. 2b). Such cracks may increase the mechanical interlock between the HAp coating and the Ti substrate, thereby increasing the adhesion strength. A closer look at the crack edges showed that they were not smooth, but had a needle morphology, which was also observed in AFM images. Terraces and aggregates of nanocrystals were observed on the surface. The H_2O_2 pretreatment (denoted hereafter as H_2O_2-Ti) did not mask the original grinding grooves (Fig. 2c), but made them shallower, which means that the newly formed surface layer was much thinner than that formed during the NaOH pretreatment.

In wet coating processes, a low water contact angle (i.e. high hydrophilicity) is usually favourable in order to achieve high surface coverage. The typical shape of water drops on each of the three types of surface is demonstrated in Fig. 3. Fig. 4 includes quantitative analysis of all observations. From this figure it is evident that all three types of surface may be classified as "hydrophilic". However, both chemical pretreatments reduced the water contact angle significantly, towards the spreading/full wettability limit. If water contact angle was the only criterion for selection, then, according to Fig. 4, the H_2O_2 pretreatment would be favourable compared to the NaOH pretreatment. However, as discussed below, a pronounced surface roughness effect led to another conclusion.

The surface roughness of a metal substrate may affect significantly both the structure and properties of an electrodeposit being formed on it and the interaction between the metal surface and biological matter. The amplitude parameters most often used in the literature are the mean roughness R_a and the root-mean-square roughness Z_{rms} [38]. The mean R_a values, for example, were 13.6, 11.0 and 32.0 nm for Gr-Ti, H_2O_2-Ti and NaOH-Ti, respectively. However, matching the R_a and Z_{rms} values of HAp-coated samples with ESEM images of the same samples, it became apparent that the use of these amplitude parameters to characterize the porous coating resulted in inconsistent, misleading conclusions. The insensitivity of these two parameters has been observed before [39].

Two alternative texture parameters were found more reliable in the present work. The developed interfacial area ratio *Sdr* reflects the additional surface area contributed by the texture compared to a totally flat sampling plane. This

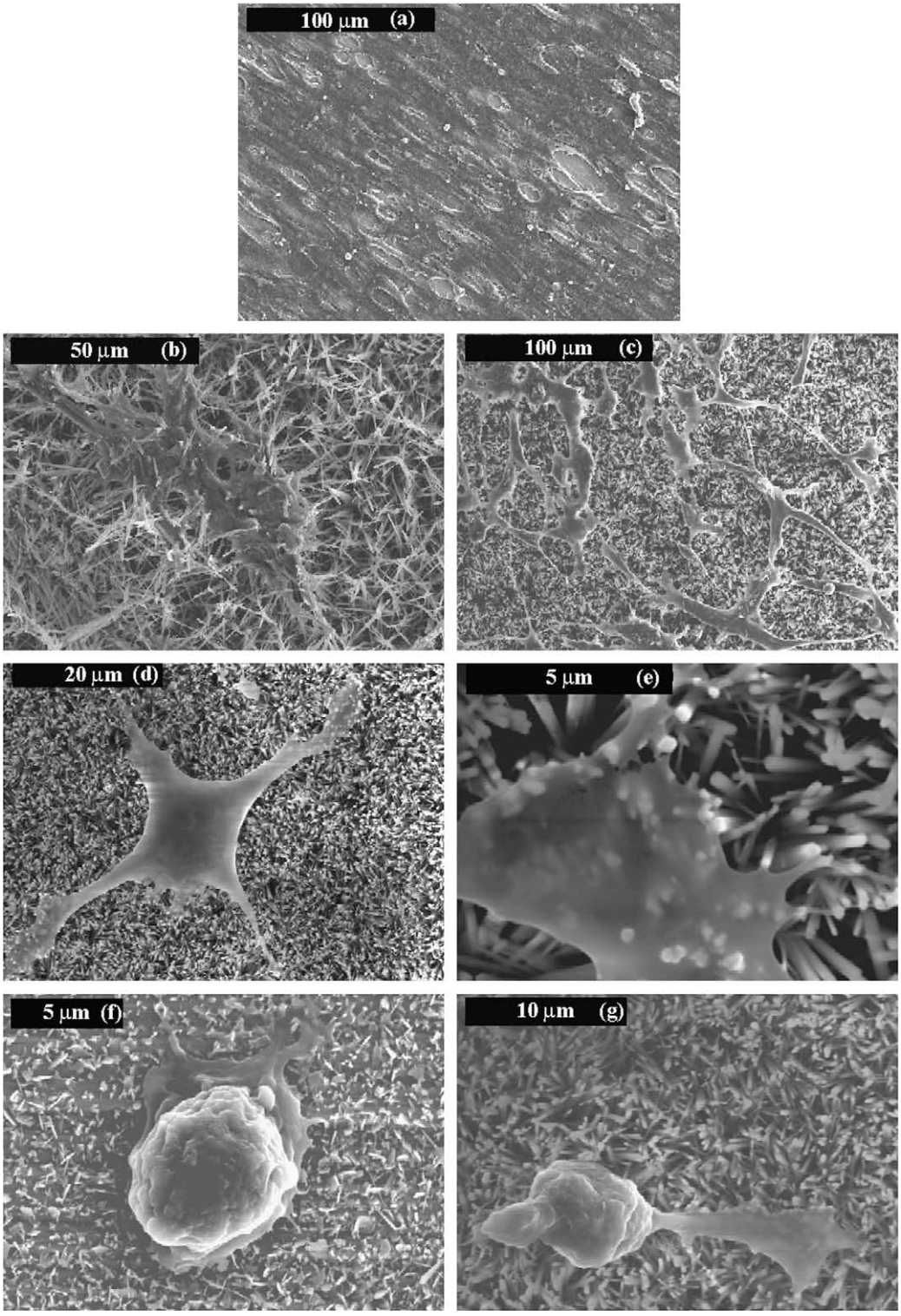

Fig. 1. SEM/ESEM images of cells on surfaces of: (a) Gr-Ti, (b and f) HAp4.2 and (c–e and g) HAp6.0.

hybrid parameter can be useful in applications involving surface coatings and adhesion, or when considering surfaces used with lubricants and other fluids. The core fluid retention index *Sci* is derived from the bearing area analysis of the complete three-dimensional surface. It is a measure, relative to Z_{rms}, of the volume of fluid that the surface would support from 5% to 80% of the bearing area [39,40]. Both *Sdr* and *Sci* were determined by the SPIP™ image processing software applied to AFM images.

According to Fig. 4, NaOH-Ti had a much higher *Sdr* value compared to either Gr-Ti or H_2O_2-Ti. This means that, at least from a texture point of view, NaOH-Ti would

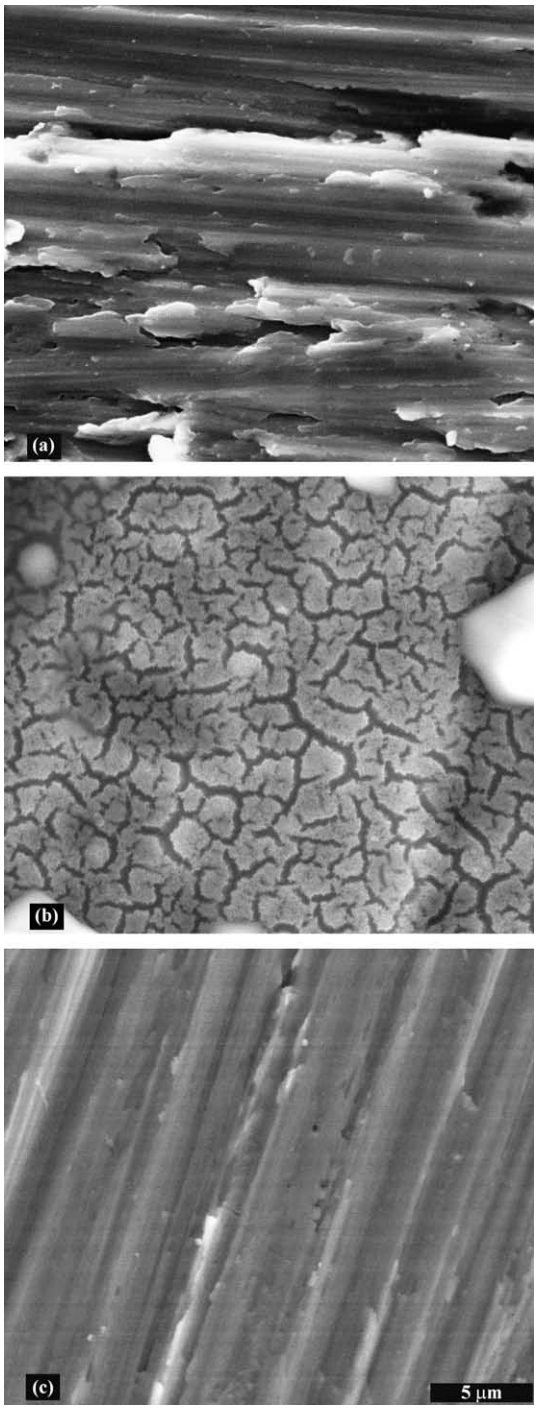

Fig. 2. ESEM images of the surfaces of (a) Gr-Ti, (b) NaOH-Ti and (c) H_2O_2-Ti.

be the favourable substrate for electrochemically deposited HAp, potentially providing higher adhesion strength. ANOVA calculation revealed that there was statistically significant difference between surface treatments with respect to the resulting *Sdr* and water contact angle values ($P = 7.3 \times 10^{-8}$ and $P = 7.2 \times 10^{-6}$, respectively). The Tukey post hoc test revealed that in the case of the *Sdr* values, all three groups were significantly different from each other ($P \leqslant 4.8 \times 10^{-3}$). In the case of the water contact angle values, this post hoc test revealed that the groups with significant difference between each other were Gr-Ti vs. H_2O_2-Ti ($P = 8.9 \times 10^{-6}$) and Gr-Ti vs. NaOH-Ti ($P = 2.3 \times 10^{-5}$), whereas H_2O_2-Ti vs. NaOH-Ti was not significantly different ($P = 0.11$). Based on these results, it was decided to focus on the NaOH pretreatment in the following in vivo study [13].

3.3. The effect of pretreatments on the electrodeposited HAp

Fig. 5 shows the typical current density transients monitored during potentiostatic deposition of HAp. The transient for HAp on Gr-Ti (denoted as Gr-Ti-HAp) is similar to that reported and analyzed before by Eliaz et al. [8,10,11]. The shape of the transients for HAp on both NaOH-Ti (denoted hereafter as NaOH-Ti-HAp) and H_2O_2-Ti (denoted as H_2O_2-Ti-HAp) was markedly different from that for Gr-Ti. In Section 3.2 it was shown that each of the three substrates had different characteristics with respect to surface texture and wettability, both of which may affect the electrodeposition process. The measured open-circuit potential (OCP) values were also significantly different: −84, −256 and −428 mV vs. SCE for H_2O_2-Ti, Gr-Ti and NaOH-Ti, respectively. Figs. 6 and 7 show that the surface morphologies of the resulting HAp coatings were also significantly different.

Fig. 6 reveals that both Gr-Ti-HAp and NaOH-Ti-HAp coatings consisted of needles (or whiskers). For the NaOH pretreatment (Fig. 6b), these needles were arranged in aggregates with a more distinct preferred orientation. ESEM images acquired at high magnification revealed that the needles were actually prismatic hexagonal bars, approximately 300 nm in diameter (Fig. 6d). Often, the outer shape of a crystal, as observed by electron microscopy, is related to the point group symmetry to which the crystal belongs. Thus, it is likely that each bar in Fig. 6d is a single crystal of HAp. The H_2O_2-Ti-HAp coating exhibited a platelet morphology (Fig. 6c), but the size of each platelet was much larger and the visual porosity level seemed to be dramatically higher. AFM images further supported this observation (see Fig. 7).

AFM images show that each Gr-Ti-HAp bar was of the order of 600 × 1120 nm laterally (Fig. 7a), while NaOH-Ti-HAp bars were smaller—of the order of 350 × 950 nm (Fig. 7b). In the case of H_2O_2-Ti-HAp, the platelets were much larger—of the order of several micrometers (Fig. 7c). The bar/platelet dimensions measured in this work are more than one order of magnitude larger than the crystal sizes known for HAp in the human body [41]. The reason for this difference has been explained elsewhere [8]. When imaging the structure shown in Fig. 7b at even higher magnification (Fig. 7d), it became apparent that each terrace was not equiaxed, but rather consisted of many small fibers with elliptic-like cross-section, stacked together. Each fiber was approximately 25–50 nm in its largest diameter. This is already the size scale typical of biological HAp crystals.

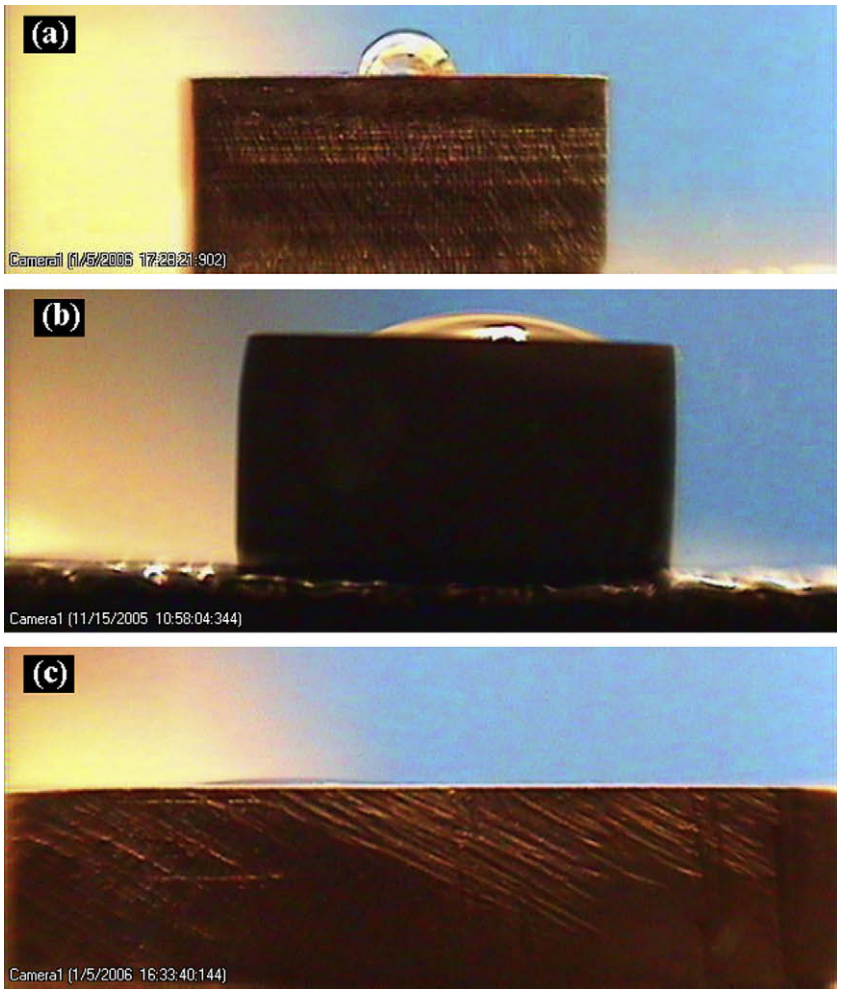

Fig. 3. Water drops on different surfaces: (a) Gr-Ti, (b) NaOH-Ti and (c) H_2O_2-Ti. (c) was magnified digitally in order to enable identification of the drop.

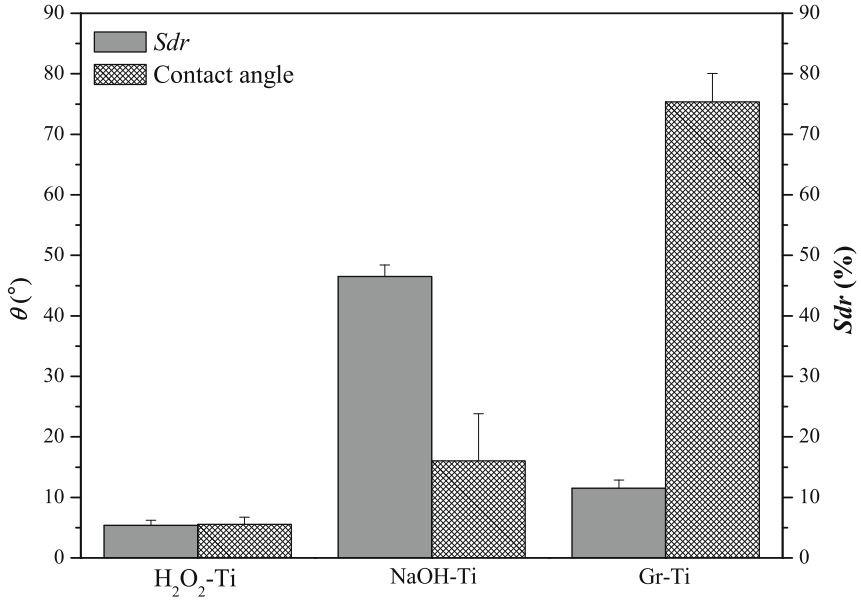

Fig. 4. Roughness and water contact angle of pretreated titanium surfaces. The data are presented as means ± standard deviation.

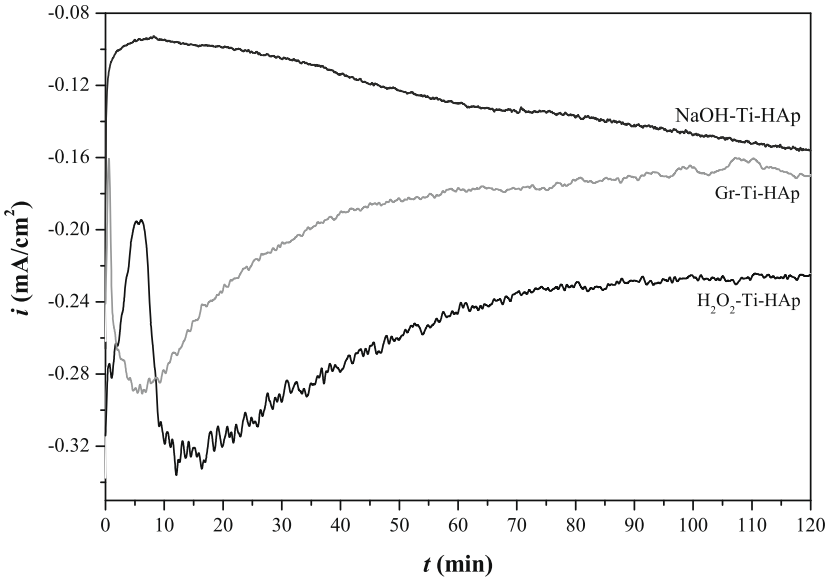

Fig. 5. The typical current density transients during potentiostatic deposition of HAp on three types of substrate.

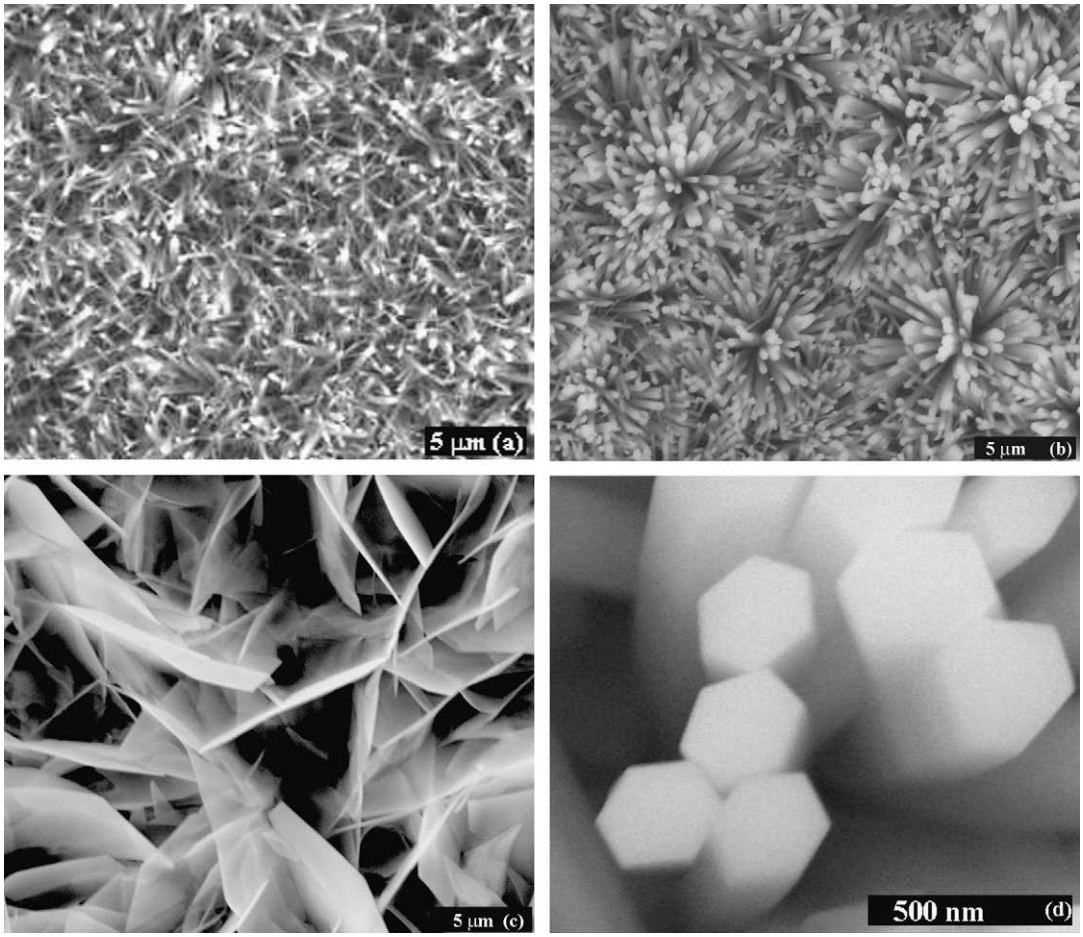

Fig. 6. ESEM images revealing the typical surface morphologies of: (a) Gr-Ti-HAp, (b) NaOH-Ti-HAp and (c) H_2O_2-Ti-HAp. High-magnification image (d) shows that the bars in (b) have hexagonal cross-section.

The measured values of the texture parameters *Sdr* and *Sci* for the HAp-coated samples are presented in Fig. 8 in comparison to those of Gr-Ti. These values are based on AFM data. It is evident that NaOH-Ti-HAp had the highest roughness. Therefore, from the roughness point of view, it may be expected that this surface would be the preferred

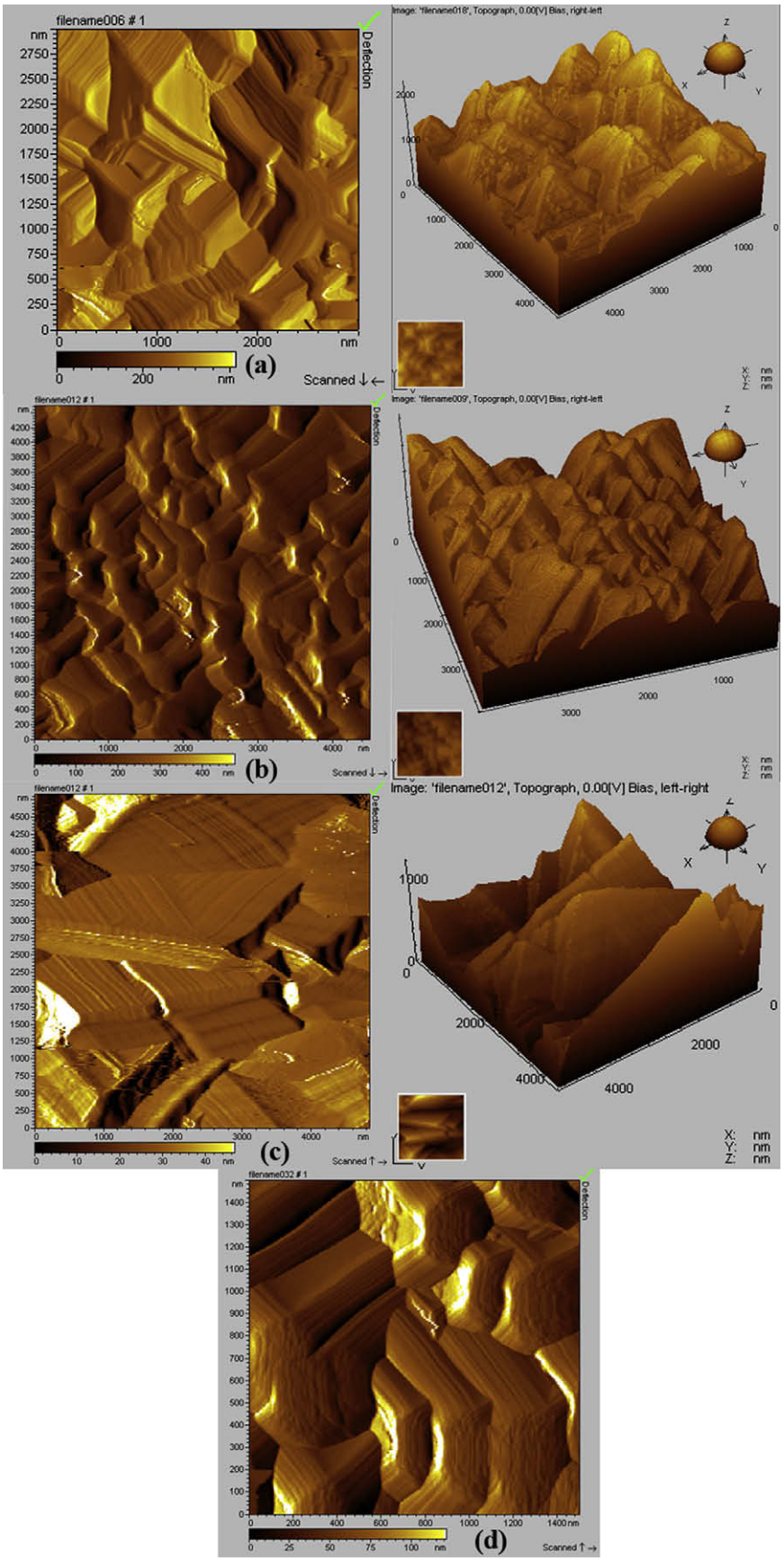

Fig. 7. AFM deflection and three-dimensional images revealing the typical morphologies of: (a) Gr-Ti-HAp, (b) NaOH-Ti-HAp and (c) H_2O_2-Ti-HAp. High-magnification deflection image (d) shows that the terraces in (b) represent stacking of fibers with elliptic-like cross-section.

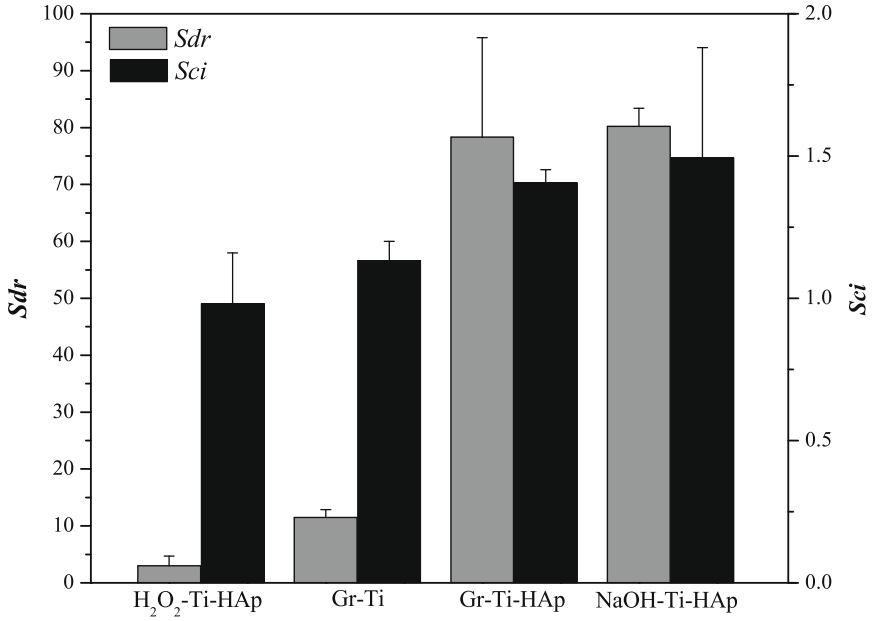

Fig. 8. The measured developed interfacial ratio (*Sdr*) and core fluid retention index (*Sci*) of uncoated vs. HAp-coated samples. The data are presented as means ± standard deviation.

one for osteoblastic cells to adhere onto. ANOVA calculation showed that the *Sci* values were not significantly different between groups ($P = 6.6 \times 10^{-2}$). Significant difference between the four types of samples was observed with respect to the *Sdr* values ($P = 5.8 \times 10^{-6}$). The Tukey post hoc test revealed that the groups with significant difference between each other were Gr-Ti vs. Gr-Ti-HAp ($P = 7.7 \times 10^{-5}$), Gr-Ti vs. NaOH-Ti-HAp ($P = 6.3 \times 10^{-5}$), H_2O_2-Ti-HAp vs. Gr-Ti-HAp ($P = 3.2 \times 10^{-5}$) and H_2O_2-Ti-HAp vs. NaOH-Ti-HAp ($P = 2.6 \times 10^{-5}$). The values for Gr-Ti vs. H_2O_2-Ti-HAp ($P = 0.66$) and Gr-Ti-HAp vs. NaOH-Ti-HAp ($P = 0.99$) were not significantly different. It seems that *Sdr* was more sensitive than *Sci* in identifying statistical differences between the four groups.

The cells' morphology on pretreated and electrodeposited samples was similar to that presented in Fig. 1 for HAp6.0. Fig. 9 shows the digital cell counts per area unit (partial population). Two typical fluorescence images of the cell nuclei (Hoechst staining) are also included. The highest number of cells was counted on NaOH-Ti-HAp, while the lowest number was observed on Gr-Ti. ANOVA calculation showed significant difference between the four groups of samples ($P = 4.2 \times 10^{-23}$). The Tukey post hoc test revealed that all groups were significantly different from one another ($P \leqslant 9.8 \times 10^{-4}$).

3.4. The effect of electron-beam treatment

Modification of the surface energy on the nanoscale was made both to HAp-coated and to uncoated samples, applying the process developed by Rosenman et al. [27–31]. The results of a feasibility study are presented here. Gr-Ti and Gr-Ti-HAp, which were originally hydrophilic, were treated to become hydrophobic (denoted hereafter as Gr-Ti-hpb and Gr-Ti-HAp-hpb, respectively). Gr-Ti was also treated under UV illumination to render it even more hydrophilic (denoted as Gr-Ti-hpl). Untreated Gr-Ti and Gr-Ti-HAp served as controls.

Cell count revealed that the highest cell density was on Gr-Ti-HAp (Fig. 10). Therefore, all other cell count values in Fig. 10 were normalized relative to this value. For uncoated Ti it is evident that the electron-beam treatment resulted in an increase in the cell density, either for Gr-Ti-hpl or for Gr-Ti-hpb, although the increase was more significant in the case of Gr-Ti-hpl. When the most hydrophilic Gr-Ti-HAp was post-treated, its water contact angle increased dramatically and the cell density decreased. Interestingly, the cell density on Gr-Ti-HAp-hpb was nearly the same as on Gr-Ti-hpl. Based on Fig. 10 it is concluded that the good bioactivity of the electrodeposited HAp could result from a synergistic effect of texture and hydrophilicity.

4. Discussion

As mentioned in Section 3.1, the HAp6.0 coating was both richer in Ca and more crystalline than HAp4.2. HAp6.0 was also more bioactive; the cells on it were stretched and exhibited more lamellipodia and filopodia. In contrast, cells on Gr-Ti were flattened and exhibited "contact guidance". It is well known that the crystallinity of a biomaterial surface affects specific cell responses such as the organization of cytoskeleton filaments and cell proliferation mechanisms. Spreading of osteoblasts, for example, has been reported to be faster on more crystalline surfaces, mainly due to the development of a more organized cytoskeleton [42]. During cell culture, extracellular

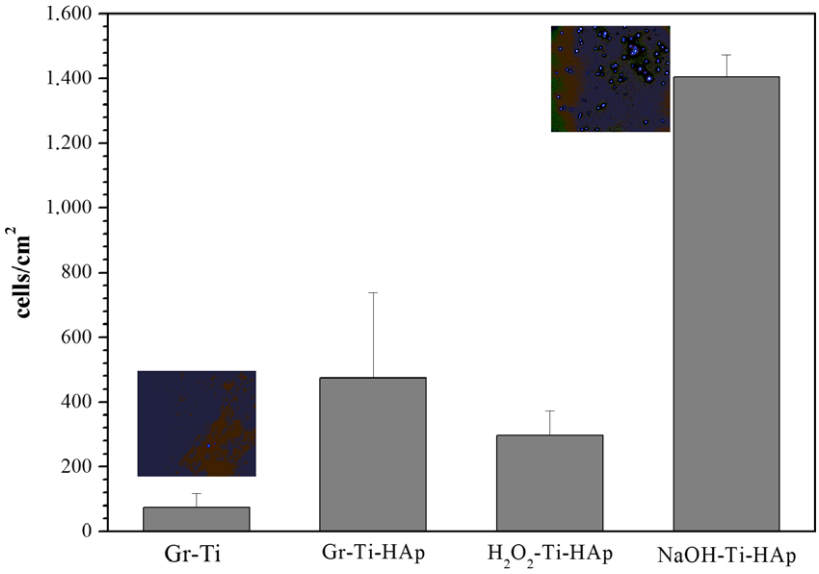

Fig. 9. Cell density on different surfaces (partial population). The data are presented as means ± standard deviation. Inset: Two typical fluorescent images of cell nuclei (Hoechst staining) on Gr-Ti vs. NaOH-Ti-HAp.

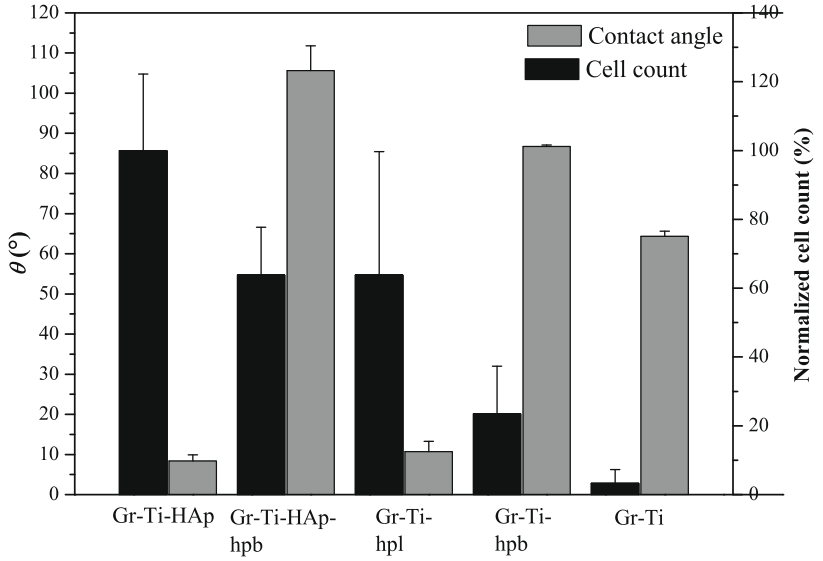

Fig. 10. Normalized cell count and water contact angle for several uncoated and HAp-coated surfaces. The data are presented as means ± standard deviation.

matrix (and other) proteins adsorb onto the biomaterial surface and help in the subsequent cell attachment. In the case of osteoblast culture in serum, which is relevant to the present study, fibronectin and vitronectin are two important proteins that affect the cell attachment and spreading [43,44]. It has been reported that calcium ions in HAp, which form sites of positive charge, aid the adhesion of these two proteins, thus promoting the attachment of osteoblasts [45,46]. Other researchers have also reported the positive effect of calcium ions on cell growth [47,48], in contrast to the inhibitory effect of phosphate ions on cell activity [49]. Thus, the enhanced bioactivity of HAp6.0 compared to HAp4.2 may be explained in the combined effect of crystallinity and Ca content.

In this work, the attachment of cells was studied. This process occurs rapidly and involves short-term events such as physicochemical linkages between cells and materials, relevant ionic forces, van der Waals forces, etc. [23,50]. The longer-term process of adhesion was not studied. The use of medical devices involves interactions between the surface of the devices and cells. The initial interactions are important towards the processes of cell proliferation and differentiation of a desired tissue when integrating with the implant. The initial cell attachment will allow the sig-

nalling process that controls cell viability and proliferation capacity. Structural features of the material have been shown to modulate the nature of MBA-15 osteogenic cell attachment and the resulting cell shape and to affect cell proliferation, differentiation or apoptosis decisions, even within 24 h of cell culturing [51].

Cell motility is generally associated with the protrusion of two types of actin-rich structures, namely lamellipodia and filopodia, at the leading edge of migrating or spreading cells [52]. These focal contacts serve as coordination sites between cell adhesion and motility; enhanced focal adhesion is associated with reduced cell motility. The elongation and reorientation of filopodia may be determined by guidance cues from the environmental signalling, e.g. the biomaterial surface structure [53,54]. From Fig. 1 it is evident that the osteoblastic cells had more enhanced motility on HAp6.0 than on Gr-Ti. The morphology of flattened cells with numerous filopodia is similar to that reported elsewhere for osteoblasts on CaP [55,56]. The phenomenon reflected, for example, by anchorage of actin fibers at the periphery of artificial pillars where focal contacts form and stretch from one pillar to the next was termed "topographical compensation" or "gap guidance" [57]. Regarding the behaviour of cells on Gr-Ti, it is well known that, in response to microgrooved surfaces, cells may elongate in the direction of the grooves and be travel-guided by them. This phenomenon has become known as "contact guidance" [36,37,58–60]. The groove depth was shown to be much more important than the spacing between grooves in determining cell alignment, which increased with depth [58].

In Section 3.2 it was shown that the NaOH pretreatment resulted in the roughest substrate surface in terms of *Sdr*. Hence, it was expected that this pretreatment would provide the highest adhesion strength to the HAp coating. Indeed, in a recent study (unpublished data) Eliaz et al. found that the adhesion strength of grit-blasted Ti was the highest when NaOH treatment was added (19.6 MPa), but lower when the H_2O_2 treatment was used instead (7.2 MPa). In comparison, HAp on Gr-Ti (with no grit blast) exhibited the lowest adhesion strength (2.1 MPa). In the present study, after electrodeposition, NaOH-Ti-HAp was the roughest in terms of *Sdr* (Fig. 8) and had the highest cell coverage (Fig. 9). In a recent in vivo study [13], the soaking of Ti–6Al–4V in NaOH, without subsequent heat treatment, provided both enhanced osseointegration and reduced occurrence of delamination compared to grit-blasted, grit-blasted and electrodeposited, and plasma-sprayed implants. It was hypothesized that the higher measured content of the octacalcium phosphate phase in NaOH-Ti-HAp and the associated increase in the solubility of this coating in vivo were responsible for the enhanced osseointegration. Yet, the NaOH treatment was found beneficial also in the case of the uncoated implant [13]. The results in the present in vitro study are in accordance with that in vivo study. In addition, the effects of both roughness and hydrophilicity are demonstrated.

The effect of roughness on cell attachment has been demonstrated before [23,36,43,50,58,61]. It was shown that the surface roughness must be within the scale of the cell to be perceived by the cell, and within this limit, rougher surfaces support the expression of a more differentiated osteoblastic phenotype based on increased alkaline phosphatase activity and osteocalcin production [50]. It was also reported that increased surface roughness, both at the micrometer and at the nanometer levels, without changes in surface chemistry, could promote functions of osteoblasts, leading to new bone synthesis [61]. Most studies, however, have expressed the roughness in terms of R_a. It is usually ignored that R_a (as Z_{rms}) may be misleading, giving, for example, identical values to two surfaces that are (microscopically) clearly different [39]. Fig. 8 shows the following descending order of *Sdr*: NaOH-Ti-HAp > Gr-Ti-HAp > Gr-Ti > H_2O_2-Ti-HAp. This order is supported by Figs. 6 and 7. On the other hand, R_a analysis of the same raw data (AFM) resulted in the following descending order of roughness: Gr-Ti-HAp > NaOH-Ti-HAp > H_2O_2-Ti-HAp > Gr-Ti. This, of course, could have led to a wrong explanation!

The adhesion and proliferation of osteoblasts have been correlated with substratum wettability, the cells exhibiting a strong preference for hydrophilic substrata [22]. Fig. 10 (Section 3.4) allows for isolation of the effect of surface energy (or, surface charge) per se, because the electron-beam post-treatment changes neither the surface morphology and roughness nor the chemistry of the surface (except, maybe, formation of a carbon-rich contamination layer [31]). Comparison between Gr-Ti-HAp and Gr-Ti-HAp-hpb, Gr-Ti-hpb and Gr-Ti-hpl, Gr-Ti-hpl and Gr-Ti-HAp-hpb, supports the claim for the positive effect of hydrophilicity. Kelvin probe measurements showed that the different uncoated and HAp-coated surfaces had different surface charges. It should be borne in mind, however, that when relating the relative biological interaction with surface energy, there may be an optimal biocompatibility zone with respect to the critical surface tension (or surface free energy) [62]. Therefore, further study should be carried out, in which the surface energy will be tuned in a controlled manner from full spreading to superhydrophobicity, taking advantage of the unique electron-beam process, and the resulting interaction of cells with the surface will be analyzed. It has been reported that the water contact angle increases monotonically with the incident charge dose [31]. In addition, it may be possible to distinguish between the contributions of the Lifshitz–van der Waals forces of attraction and repulsion attributed to long-range forces and of the short-range polar interactions of Lewis acid/base type to the total free energy of the surface [31].

5. Conclusions

The effect of surface pretreatments (i.e. grinding, NaOH treatment and H_2O_2 treatment), surface post-treatment (electron-beam irradiation) and bath pH (either 6 or 4.2)

on the surface texture, water contact angle and interaction with bone-forming cells of electrochemically deposited HAp coating on CP-Ti was studied. HAp electrodeposited at pH 6 was preferable compared to HAp electrodeposited at pH 4.2 with respect to osteoblast cell attachment, because the former coating was both richer in Ca and more crystalline. NaOH pretreatment resulted in the roughest substrate surface and in the highest adhesion strength of the HAp coating. The HAp coating after NaOH pretreatment was the roughest and had the highest cell coverage. The use of the amplitude parameters R_a (mean roughness) and Z_{rms} (root-mean-square roughness) might lead to misleading conclusions, particularly when studying porous coatings such as HAp. The use of the hybrid parameter *Sdr* (developed interfacial area ratio) was found to be more sensitive and reliable in distinguishing between different surfaces and predicting their effect on cell attachment. The use of the electron-beam post-treatment demonstrated the preference of osteoblasts for hydrophilic surfaces. This treatment provides a new opportunity for isolating the effect of surface charge/energy per se. The HAp crystals on NaOH-treated surface were similar in their hexagonal morphology and size to the biological apatite. Elliptical fibers were stacked together, forming non-equiaxed terraces within each bar. The electrodeposited HAp enhanced the cell attachment, compared to the CP-Ti substrate.

Acknowledgements

The authors thank Mario Levinshtein and Oshrit Ritman from the Biomaterials and Corrosion Laboratory for their technical and statistical analysis work, respectively. We also thank Zahava Barkay from the Wolfson Applied Materials Research Centre for her help with the ESEM characterization.

References

[1] Furlong RJ, Osborn JF. Fixation of hip prostheses by hydroxyapatite ceramic coatings. J Bone Joint Surg Br 1991;73:741–5.
[2] Campbell AA. Bioceramics for implant coatings. Mater Today 2003; 6:26–30.
[3] Jaffe WL, Scott DF. Total hip arthroplasty with hydroxyapatite-coated prostheses. J Bone Joint Surg Am A 1996;78:1918–34.
[4] Soballe K, Overgaard S. The current status of hydroxyapatite coating of prostheses. J Bone Joint Surg Br B 1996;78:689–91.
[5] Munting E. The contributions and limitations of hydroxyapatite coatings to implant fixation—a histomorphometric study of load bearing implants in dogs. Int Orthop 1996;20:1–6.
[6] Eliaz N, Sridhar TM, Kamachi Mudali U, Baldev Raj. Electrochemical and electrophoretic deposition of hydroxyapatite for orthopaedic applications. Surf Eng 2005;21:238–42.
[7] Wang H, Eliaz N, Xiang Z, Hsu HP, Spector M, Hobbs LW. Early bone apposition in vivo on plasma-sprayed and electrochemically deposited hydroxyapatite coatings on titanium alloy. Biomaterials 2006;27:4192–203.
[8] Eliaz N, Eliyahu M. Electrochemical processes of nucleation and growth of hydroxyapatite on titanium supported by real-time electrochemical atomic force microscopy. J Biomed Mater Res A 2007;80:621–34.
[9] Eliaz N, Kopelovitch W, Burstein L, Kobayashi E, Hanawa T. Electrochemical processes of nucleation and growth of calcium phosphate on titanium supported by real-time quartz crystal microbalance measurements and X-ray photoelectron spectroscopy analysis. J Biomed Mater Res A 2009;89:270–80.
[10] Eliaz N. Electrocrystallization of calcium phosphates. Isr J Chem 2008;48:159–68.
[11] Eliaz N, Sridhar TM. Electrocrystallization of hydroxyapatite and its pH dependence. Cryst Growth Des 2008;8:3965–77.
[12] Eliaz N. Electrochemical modification of biomaterial surfaces. In: Karlinsey RL, editor. Recent developments in advanced medical and dental materials using electrochemical methodologies. Trivandrum, India: Research Signpost, in press.
[13] Lakstein D, Kopelovitch W, Barkay Z, Bahaa M, Hendel D, Eliaz N. Enhanced osseointegration of grit-blasted, NaOH-treated and electrochemically hydroxyapatite-coated Ti–6Al–4V implants in rabbits. Acta Biomater 2009;5:2258–69.
[14] Kokubo T, Miyaji F, Kim HM. Spontaneous formation of bonelike apatite layer on chemically treated titanium metals. J Am Ceram Soc 1996;79:1127–9.
[15] Kim HM, Miyaji F, Kokubo T, Nakamura T. Effect of heat treatment on apatite-forming ability of Ti induced by alkali treatment. J Mater Sci Mater Med 1997;8:341–7.
[16] Kokubo T. Apatite formation on surfaces of ceramics, metals and polymers in body environment. Acta Mater 1998;46:2519–27.
[17] Chosa N, Taira M, Saitoh S, Sato N, Araki Y. Characterization of apatite formed on alkaline-heat-treated Ti. J Dent Res 2004;83:465–9.
[18] Park JH, Lee DY, Oh KT, Lee YK, Kim KN. Bioactive calcium phosphate coating on sodium hydroxide-pretreated titanium substrate by electrodeposition. J Am Ceram Soc 2004;87:1792–4.
[19] Bearinger JP, Orme CA, Gilbert JL. Effect of hydrogen peroxide on titanium surfaces: in situ imaging and step-polarization impedance spectroscopy of commercially pure titanium and titanium, 6-aluminum, 4-vanadium. J Biomed Mater Res A 2003;67:702–12.
[20] Park JH, Lee YK, Kim KM, Kim KN. Bioactive calcium phosphate coating prepared on H_2O_2-treated titanium substrate by electrodeposition. Surf Coat Technol 2005;195:252–7.
[21] Rohanizadeh R, Al-Sadeq M, LeGeros RZ. Preparation of different forms of titanium oxide on titanium surface: effects on apatite deposition. J Biomed Mater Res A 2004;71:343–52.
[22] Lim JY, Liu XM, Vogler EA, Donahue HJ. Systematic variation in osteoblast adhesion and phenotype with substratum surface characteristics. J Biomed Mater Res A 2004;68:504–12.
[23] Anselme K. Osteoblast adhesion on biomaterials. Biomaterials 2000;21:667–81.
[24] Mrksich M, Whitesides GM. Using self-assembled monolayers to understand the interactions of man-made surfaces with proteins and cells. Annu Rev Biophys Biomol Struct 1996;25:55–78.
[25] Ichimura K, Oh SK, Nakagawa M. Light-driven motion of liquids on a photoresponsive surface. Science 2000;288:1624–6.
[26] Gallardo BS, Gupta VK, Eagerton FD, Jong LI, Craig VS, Shah RR, et al. Electrochemical principles for active control of liquids on submillimeter scales. Science 1999;283:57–60.
[27] Rosenman G, Aronov D, Dekchtiar Yu. Method and device for wettability modification of materials. PCT Application WO 2007/049280; 2007.
[28] Aronov D, Rosenman G, Karlov A, Shashkin A. Wettability patterning of hydroxyapatite induced by surface potential modification. Appl Phys Lett 2006;88:163902.
[29] Aronov D, Rosen R, Ron EZ, Rosenman G. Tunable hydroxyapatite wettability: effect on adhesion of biological molecules. Process Biochem 2006;41:2367–72.
[30] Aronov D, Rosenman G. Trap state spectroscopy studies and wettability modification of hydroxyapatite nanobioceramics. J Appl Phys 2007;101:34701.
[31] Aronov D, Rosen R, Ron EZ, Rosenman G. Electron-induced surface modification of hydroxyapatite-coated implant. Surf Coat Technol 2008;202:2093–102.

[32] Kwok DY, Neumann AW. Contact angle measurement and contact angle interpretation. Adv Colloid Interface Sci 1999;81:167–249.
[33] Benayahu D, Kletter Y, Zipori D, Wientroub S. Bone marrow-derived stromal cell-line expressing osteoblastic phenotype in vitro and osteogenic capacity in vivo. J Cell Physiol 1989;140:1–7.
[34] Benayahu D, Kompier R, Shamay A, Kadouri A, Zipori D, Wientroub S. Mineralization of marrow-stromal osteoblasts MBA-15 on three-dimensional carriers. Calcif Tissue Int 1994;55:120–7.
[35] Deng Y, Zhao K, Zhang XF, Hub P, Chen GQ. Study on the three-dimensional proliferation of rabbit articular cartilage-derived chondrocytes on polyhydroxyalkanoate scaffolds. Biomaterials 2002; 23:4049–56.
[36] Anselme K, Bigerelle M, Noel B, Dufresne E, Judas D, Iost A, et al. Qualitative and quantitative study of human osteoblast adhesion on materials with various surface roughnesses. J Biomed Mater Res 2000;49:155–66.
[37] Matsuzaka K, Walboomers XF, Yoshinari M, Inoue T, Jansen JA. The attachment and growth behavior of osteoblast-like cells on microtextured surfaces. Biomaterials 2003;24:2711–9.
[38] Eliaz N, Nissan O. Innovative processes for electropolishing of medical devices made of stainless steels. J Biomed Mater Res A 2007;83:546–57.
[39] Glossary of surface texture parameters. Michigan metrology. Online. 2008 November. Available from: http://www.michmet.com/S_Parameters.htm.
[40] Stout KJ, Sullivan PJ, Dong WP, Mainsah E, Luo N, Mathia T, et al. The development of methods for characterization of roughness in three dimensions, EUR 15178 EN of Commission of the European Communities. Birmingham: University of Birmingham; 1993.
[41] Ratner BD, Hoffman AS, Schoen FJ, Lemons JE. Biomaterials science: an introduction to materials in medicine. San Diego (CA): Academic Press; 2004, p. 163–5.
[42] Ball MD, Downes S, Scotchford CA, Antonov EN, Bagratashvili VN, Popov VK, et al. Osteoblast growth on titanium foils coated with hydroxyapatite by pulsed laser ablation. Biomaterials 2001;22: 337–47.
[43] Narayanan R, Kim SY, Kwon TY, Kim KH. Nanocrystalline hydroxyapatite coatings from ultrasonated electrolyte: preparation, characterization, and osteoblast responses. J Biomed Mater Res A 2008;87:1053–60.
[44] Benayahu D, Fried A, Efraty M, Robey PG, Wientroub S. Bone marrow interface: preferential attachment of an osteoblastic marrow stromal cell line. Cell Biochem 1995;59:151–60.
[45] Feng B, Weng J, Yang BC, Qu SX, Zhang XD. Characterization of titanium surfaces with calcium and phosphate and osteoblast adhesion. Biomaterials 2004;25:3421–8.
[46] Zhu X, Son DW, Ong JL, Kim KH. Characterization of hydrothermally treated anodic oxides containing Ca and P on titanium. J Mater Sci Mater Med 2003;14:629–34.
[47] Cheung HS, Story MT, McCarty DJ. Mitogenic effects of HA and calcium pyrophosphate dihydrate crystals on cultured mammalian cells. Arthritis Rheum 1984;27:665–74.
[48] Cheung HS, McCarty DJ. Mitogenesis induced by calcium containing crystal: role of intracellular dissolution. Exp Cell Res 1985;157:63–70.
[49] Knabe C, Gildenhaar R, Berger G, Ostapowicwz W, Fitzer R, Radlanski RJ, et al. Morphological evaluation of osteoblasts cultured on different calcium phosphate ceramics. Biomaterials 1997;18: 1339–47.
[50] Boyan BD, Lohmann CH, Dean DD, Sylvia VL, Cochran DL, Schwartz Z. Mechanisms involved in osteoblast response to implant surface morphology. Ann Rev Mater Res 2001;31:357–71.
[51] Marom R, Shur I, Solomon R, Benayahu D. Characterization of adhesion and differentiation markers of osteogenic marrow stromal cells. J Cell Physiol 2005;202:41–8.
[52] Lodish H, Berk A, Matsudaira P. Molecular cell biology. New York: Freeman & Co.; 2004, p. 821–3.
[53] Zhu X, Chen J, Scheideler L, Altebaeumer T, Geis-Gerstorfer J, Kern D. Cellular reactions of osteoblasts to micron- and submicron-scale porous structures of titanium surfaces. Cells Tissues Organs 2004;178: 13–22.
[54] Shur I, Zilberman M, Benayahu D, Einav S. Adhesion molecule expression by osteogenic cells cultured on various biodegradable scaffolds. J Biomed Mater Res A 2005;75:870–6.
[55] Olmo N, Martín AI, Salinas AJ, Turnay J, Vallet-Regí M, Lizarbe MA. Bioactive sol–gel glasses with and without a hydroxycarbonate apatite layer as substrates for osteoblast cell adhesion and proliferation. Biomaterials 2003;24:3383–93.
[56] Takebe J, Itoh S, Okada J, Ishibashi K. Anodic oxidation and hydrothermal treatment of titanium results in a surface that causes increased attachment and altered cytoskeletal morphology of rat bone marrow stromal cells in vitro. J Biomed Mater Res 2000;51:398–407.
[57] Su WT, Chu IM, Yang JY, Lin CD. The geometric pattern of a pillared substrate influences the cell-process distribution and shapes of fibroblasts. Micron 2006;37:699–706.
[58] Curtis A, Wilkinson C. Topographical control of cells. Biomaterials 1997;18:1573–83.
[59] Clark P, Connolly P, Curtis ASG, Dow JAT, Wilkinson CDW. Topographical control of cell behaviour: II. Multiple grooved substrata. Development 1990;108:635–44.
[60] Zinger O, Anselme K, Denzer A, Habersetzer P, Wieland M, Jeanfils J, et al. Time-dependent morphology and adhesion of osteoblastic cells on titanium model surfaces featuring scale-resolved topography. Biomaterials 2004;25:2695–711.
[61] Webster TJ, Ergun C, Doremus RH, Lanford WA. Increased osteoblast adhesion on titanium-coated hydroxylapatite that forms $CaTiO_3$. J Biomed Mater Res A 2003;67:975–80.
[62] Baier RE. Applied chemistry at protein interfaces. Adv Chem Ser 1975;145:1–25.